STATISTICS, OPTIMIZATION AND INFORMATION COMPUTING
Stat., Optim. Inf. Comput., Vol. **15**, January 2026, pp 711–732.
Published online in International Academic Press (www.IAPress.org)

Design of a Two-Stage Controller for Balancing and Stabilizing the Furuta Pendulum

Sebastián David Pintor-Ahumada, Camilo Esteban Pérez-Espíndola, Oscar Danilo Montoya*

Facultad de Ingeniería, Universidad Distrital Francisco José de Caldas, Bogotá D.C. 110121, Colombia

Abstract Control systems are essential for managing variables within dynamic systems, ensuring stability and performance according to criteria such as response time, reference accuracy, and disturbance rejection. This study focuses on designing a two-stage control strategy to stabilize the Furuta Pendulum in its upright position. The proposed approach integrates a Model Predictive Control (MPC) scheme with a swing-up and energy-based lifting technique, and is applied to a physical QUANSER inverted pendulum setup. The paper outlines the mathematical modeling process of the system and details how this model is incorporated into the MPC framework. To assess the effectiveness of the proposed controller, a comparative analysis is conducted against a traditional state feedback controller, both implemented on the same experimental platform. The controllers are tested under standardized reference inputs and disturbance scenarios, with performance evaluated through graphical analysis and the Integral Time Absolute Error (ITAE) index. Results demonstrate that the MPC-based control strategy outperforms the state feedback controller in terms of response speed, tracking precision, and steady-state accuracy. Notably, the MPC exhibits significant advantages during controller switching scenarios, highlighting its robustness and adaptability—features that are not achievable with the conventional state feedback approach.

Keywords Linear control, hybrid control, swing up and stabilization, Furuta pendulum, model predictive control

DOI: 10.19139/soic-2310-5070-2795

1. Introduction

In the field of control engineering, the need to stabilize and regulate systems with complex dynamics has driven the development of advanced control techniques [1]. A widely used benchmark for validating such strategies is the inverted pendulum, which has served as an experimental tool in laboratories since the 1950s to test new control methodologies [2].

The inverted pendulum has gained prominence in both teaching and research due to its affordability and resemblance to industrial systems. Research findings derived from it can be adapted to more robust applications, such as mobile robots, spacecraft, submarines, and electrical systems [3].

Over the years, structural variations of the inverted pendulum have emerged, including the Furuta pendulum, designed by Dr. Katuhisa Furuta in 1992 [4]. Unlike the conventional inverted pendulum, which moves linearly along a rail, the Furuta pendulum features a rotational base, introducing dynamic couplings and physical constraints that increase the complexity of its control [5]. These characteristics have made the Furuta pendulum a reference platform for evaluating control strategies applied to nonlinear systems [1].

Originally, its creator (i.e., Dr. Katuhisa Furuta) addressed the challenge of pendulum stabilization through the combination of three components that remain fundamental when designing control schemes for the Furuta pendulum. The first consists of a swing-up controller, whose purpose is to bring the pendulum close to the equilibrium region; the second is a switch that executes the transition between control actions applied to the

*Correspondence to: O. D. Montoya (Email: odmontoyag@udistrital.edu.co). Facultad de Ingeniería, Universidad Distrital Francisco José de Caldas, Bogotá D.C. 110121, Colombia

ISSN 2310-5070 (online) ISSN 2311-004X (print)

system once certain conditions on the pendulum's position are met; and the third is a stabilizer composed of an observer–regulator, which stabilizes the pendulum at the equilibrium point and applies corrective actions in response to disturbances [2]. Historically, these three components have undergone modifications depending on the specific approach taken to address the contextual control problem.

Swing-up control has evolved through various implementations, ranging from Lyapunov-based and energy-based methods—where stabilization is achieved by adjusting the system's total energy without accounting for friction [6]—to feedback compensation strategies that do not rely on Lyapunov theory [7]. Similarly, the stabilization stage has seen significant development, including heuristic techniques such as genetic algorithms for optimizing state-feedback gains [8], fuzzy controllers that partition the state space into action regions [9]. and learning-based approaches like iterative learning control [10] and artificial neural networks for system behavior prediction [11],These methods address both complex dynamics and more conventional control scenarios, such as basic state-feedback control[12, 13].

Although state-feedback control is effective for maintaining equilibrium and rejecting disturbances, it does not prioritize time optimization. This is critical, as prolonged stabilization can be detrimental to both the process and the system itself. According to[14] stabilization times and energy consumption under state-feedback control can be excessive, prompting the need for more advanced controllers to reduce response time and enhance stability at the equilibrium point.

One of the most promising strategies in this context is Model Predictive Control (MPC), which anticipates system behavior and control actions over a prediction horizon by minimizing or maximizing a cost function tied to a variable of interest [15]. For comparative purposes, this study employs a methodology that combines two controllers: a swing-up controller that drives the pendulum from any initial position to the stabilizer's operating region, and a stabilizer that maintains equilibrium using pole placement via state-feedback control [7, 9].

Pole selection has also been addressed in [10],], showing that previous methodologies can be replaced by heuristic algorithms to determine optimal feedback gains for improved system performance.

Based on the above, this work proposes the design and implementation of a model predictive controller aimed at improving performance over state-feedback control. Key performance indicators include reduced stabilization time and minimized reference tracking error, evaluated through a test scheme involving three experimental signals applied to both stabilization strategies using the same swing-up method. This research seeks to provide new evidence on the feasibility of MPC in highly coupled nonlinear systems and to enhance stabilization strategies in practical applications.

This paper is structured into four main sections. Section 2 describes the methodology used to develop the two-stage controller, beginning with the system's dynamic model and its linearization through to implementation. Section 3 presents the analysis and comparison of the proposed controller against the baseline strategy, evaluating both using a cumulative error index. Finally, Section 4 outlines the conclusions drawn from the study.

2. Methodology

This section outlines the implementation process of two control strategies applied to the Furuta pendulum. The development begins with system modeling, from which two control approaches are derived: state-feedback control and MPC. Both methods are complemented by an energy-based swing-up controller, resulting in hybrid control strategies. To analyze and compare the performance of the controllers, three standardized tests were defined to evaluate reference tracking and disturbance rejection. These tests allow for the observation and qualification of each strategy's response characteristics, supported by a quantitative analysis using the ITAE index as the evaluation criterion. This index assigns greater penalties to errors that persist over time.

2.1. Dynamic model of the Furuta pendulum

The Furuta pendulum is an underactuated system, meaning it has more degrees of freedom than actuators. It consists of a rotating base that influences the swing of a pendulum through a horizontal arm connected to the base [16]. The angle formed between a reference axis and the arm is denoted as θ, while the angle between the pendulum and a vertical line is denoted as α, as illustrated in Figure 1.

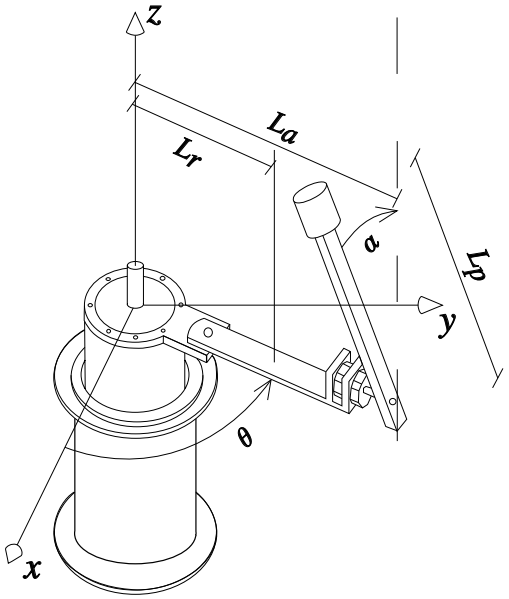

Figure 1. Furuta Pendulum Schematic. Source: [1]

To design and implement effective control over this system, it is necessary to consider its dynamics, expressed in terms of the system's input and output variables. The system dynamics are initially described using the Lagrange–Euler equations of motion (1) and (2).

$$(p_1 + p_2 \cos^2 \alpha + J_r)\,\ddot{\theta} - (p_3 \cos \alpha)\,\ddot{\alpha} + (2p_2 \sin \alpha \cos \alpha)\,\dot{\alpha}\dot{\theta} + (p_3 \sin \alpha)\,\dot{\alpha}^2 = \frac{K_t}{R_m}(V_m - K_m\dot{\theta}) - B_r\dot{\theta} \tag{1}$$

$$-(p_3 \cos \alpha)\,\ddot{\theta} + (J_p + p_2)\,\ddot{\alpha} - (p_2 \sin \alpha \cos \alpha)\,\dot{\theta}^2 - (p_4 \sin \alpha) = -B_p\,\dot{\alpha} \tag{2}$$

Where:

$$p_1 = m_p L_r^2 \tag{3}$$

$$p_2 = \frac{1}{4} m_p L_p^2 \tag{4}$$

$$p_3 = \frac{1}{2} m_p L_p L_r \tag{5}$$

$$p_4 = \frac{1}{2} m_p L_p g \tag{6}$$

Taking into account considerations (3), (4), (5) and (6) obtained as from [15], and adding to the results obtained, it is necessary to consider the resistance to motion generated by the viscosity of the shafts, considering that the motion vector is described as a function of the arm and pendulum angles $q = [\theta, \alpha]$. With this in mind, in order to establish the motion dynamics equations in a standard form, it is necessary to define the state-space equation using the notation (7).

$$x = \begin{bmatrix} x_1 \\ x_2 \\ x_3 \\ x_4 \end{bmatrix} = \begin{bmatrix} \theta \\ \dot{\theta} \\ \alpha \\ \dot{\alpha} \end{bmatrix} \tag{7}$$

In order to obtain an equation in standard form, equations (1) and (2) are rewritten in matrix form, resulting in equations (8) and (9).

$$\begin{bmatrix} d_{11} & -d_{12} \\ -d_{21} & d_{22} \end{bmatrix} \begin{bmatrix} \dot{x_2} \\ \dot{x_4} \end{bmatrix} + \begin{bmatrix} c_{11} & -c_{12} \\ -c_{21} & c_{22} \end{bmatrix} \begin{bmatrix} x_2 \\ x_4 \end{bmatrix} + \begin{bmatrix} 0 \\ g_{21} \end{bmatrix} = \begin{bmatrix} \frac{K_t}{R_m} \\ 0 \end{bmatrix} V_m \tag{8}$$

$$D \begin{bmatrix} \dot{x_2} \\ \dot{x_4} \end{bmatrix} + C \begin{bmatrix} x_2 \\ x_4 \end{bmatrix} + G = QV_m \tag{9}$$

The parameters contained in the matrices **D**, **C** and **G** are those presented in Table 1.

Table 1. Matrix coefficients of the controllable canonical form

Coefficient	Value
d_{11}	$p_1 + p_2 \cos^2 x_3 + J_r$
d_{22}	$J_p + p_2$
d_{12}, d_{21}	$p_3 \cos x_3$
c_{11}	$B_r + \dfrac{K_t K_m}{R_m}$
c_{21}	$p_2 \sin x_3 \cos x_3 \, x_2$
c_{12}	$2x_2 p_2 \sin x_3 \cos x_3 + p_3 x_4 \sin x_3$
c_{22}	B_p
g_{21}	$\dfrac{K_t K_m}{R_m}$

Equation (9) allows for straightforward isolation of the state variables contained within it, yielding the system of equations defined in Equation (10).

$$\mathbf{F}: \begin{cases} \begin{bmatrix} \dot{x}_1 \\ \dot{x}_3 \end{bmatrix} = \begin{bmatrix} x_2 \\ x_4 \end{bmatrix} \\ \begin{bmatrix} \dot{x}_2 \\ \dot{x}_4 \end{bmatrix} = \mathbf{D}^{-1} \left(\mathbf{Q} V_m - \mathbf{C} \begin{bmatrix} x_2 \\ x_4 \end{bmatrix} - \mathbf{G} \right) \end{cases} \tag{10}$$

2.1.1. Linear Model *In control system design, system dynamics are often represented using transfer functions. Although the dynamics of the Furuta pendulum are nonlinear, it is possible to linearize the system by applying the method described by the authors in [1] and [17], which involves a first-order Taylor series expansion of the state equations around the system's equilibrium point (11). In this case, the equilibrium point of interest is the unstable upright position, which the linear controller aims to reach and maintain. This linearization serves as the foundation for the controller's operation.This linearization constitutes the basis for the controller's operation; therefore, the validity and accuracy of the theoretical model from which the linear approximation is derived are crucial for the rigor and performance of the controller, such that a model lacking sufficient detail for the reference application entails additional adjustments in the controller to ensure proper functioning.*

$$\mathbb{P}_E \left\{ \bar{x} = \begin{bmatrix} \theta \\ \dot{\theta} \\ \alpha \\ \dot{\alpha} \end{bmatrix} = \begin{bmatrix} \mathbb{R} \\ 0 \\ k\pi \\ 0 \end{bmatrix}, \quad \bar{u} = [u] = [0] \right\} \quad k \in \{1, 2, 3, \ldots, n\} \tag{11}$$

The linear model is proposed in [1] as the result obtained from solving the following expression (12) ,where **F** represents the system of equations described by the state-space equations.

$$\mathbf{F}_{\text{lineal}}: \begin{bmatrix} \dot{x}_{l1} \\ \dot{x}_{l2} \\ \dot{x}_{l3} \\ \dot{x}_{l4} \end{bmatrix} = \begin{bmatrix} \left.\frac{\partial F_1}{\partial x_1}\right|_{x\to\bar{x}} & \left.\frac{\partial F_1}{\partial x_2}\right|_{x\to\bar{x}} & \left.\frac{\partial F_1}{\partial x_3}\right|_{x\to\bar{x}} & \left.\frac{\partial F_1}{\partial x_4}\right|_{x\to\bar{x}} \\ \left.\frac{\partial F_2}{\partial x_1}\right|_{x\to\bar{x}} & \left.\frac{\partial F_2}{\partial x_2}\right|_{x\to\bar{x}} & \left.\frac{\partial F_2}{\partial x_3}\right|_{x\to\bar{x}} & \left.\frac{\partial F_2}{\partial x_4}\right|_{x\to\bar{x}} \\ \left.\frac{\partial F_3}{\partial x_1}\right|_{x\to\bar{x}} & \left.\frac{\partial F_3}{\partial x_2}\right|_{x\to\bar{x}} & \left.\frac{\partial F_3}{\partial x_3}\right|_{x\to\bar{x}} & \left.\frac{\partial F_3}{\partial x_4}\right|_{x\to\bar{x}} \\ \left.\frac{\partial F_4}{\partial x_1}\right|_{x\to\bar{x}} & \left.\frac{\partial F_4}{\partial x_2}\right|_{x\to\bar{x}} & \left.\frac{\partial F_4}{\partial x_3}\right|_{x\to\bar{x}} & \left.\frac{\partial F_4}{\partial x_4}\right|_{x\to\bar{x}} \end{bmatrix} \begin{bmatrix} x_{l1} \\ x_{l2} \\ x_{l3} \\ x_{l4} \end{bmatrix} + \begin{bmatrix} \left.\frac{\partial F_1}{\partial u}\right|_{u\to\bar{u}} \\ \left.\frac{\partial F_2}{\partial u}\right|_{u\to\bar{u}} \\ \left.\frac{\partial F_3}{\partial u}\right|_{u\to\bar{u}} \\ \left.\frac{\partial F_4}{\partial u}\right|_{u\to\bar{u}} \end{bmatrix} \tag{12}$$

Using the result from equation (12) along with the QUBE Servo 2 equipment values obtained from [18], the inertia coefficients from [19], and the viscosity coefficients from [20], evaluated at the equilibrium point $[0, 0, 0, 0]^T$ the parameters of the inverted pendulum are presented in Table 2.

Table 2. QUANSER inverted pendulum parameters

Symbol	Description	Unit	Value
m_p	Mass of the pendulum arm	kg	0.0240
L_p	Mean length of the rotating base	m	0.129
L_r	Mean length of the pendulum	m	0.0850
B_r	Viscous damping coefficient of the rotating base	$\frac{\text{N·m·s}}{\text{rad}}$	0.0024
B_p	Viscous damping coefficient of the pendulum	$\frac{\text{N·m·s}}{\text{rad}}$	0.0024
g	Gravitational constant	$\frac{\text{m}}{\text{s}^2}$	9.81
J_r	Moment of inertia of the rotating base	$\text{kg} \cdot \text{m}^2$	5.72×10^{-5}
J_p	Moment of inertia of the pendulum	$\text{kg} \cdot \text{m}^2$	3.32×10^{-5}
R_m	Armature resistance of the motor	Ω	8.40
K_t	Motor torque constant	$\frac{\text{N·m}}{\text{A}}$	0.0420
K_m	Motor back-emf constant	$\frac{\text{V·s}}{\text{rad}}$	0.0420

The behavior of the Furuta pendulum in the linear region near 0,corresponding to the upright equilibrium position, is ultimately described by the following state-space equations.

$$\mathbf{F}_{\text{lineal}}: \begin{bmatrix} \dot{x}_{l1} \\ \dot{x}_{l2} \\ \dot{x}_{l3} \\ \dot{x}_{l4} \end{bmatrix} = \begin{bmatrix} 0 & 1 & 0 & 0 \\ 0 & -2.0886 & 149.2751 & 0 \\ 0 & 0 & 0 & 1 \\ 0 & -2.0643 & 261.6091 & 0 \end{bmatrix} \begin{bmatrix} x_{l1} \\ x_{l2} \\ x_{l3} \\ x_{l4} \end{bmatrix} + \begin{bmatrix} 0 \\ 49.7275 \\ 0 \\ 49.1493 \end{bmatrix} V_m \tag{13}$$

2.2. *Swing-Up Control*

To enable stabilization within the linear region, the pendulum must first be brought to a position near the upright equilibrium. This task is accomplished using a control strategy that exploits the exchange of potential energy within the pendulum system [21].

Taking Table 2 into account, and disregarding both friction and the rigidity of the pendulum body, the dynamic behavior of the pendulum is modeled by equation (14):

$$J\ddot{\alpha} - mgl \sin \alpha + ma_p l \cos \alpha = 0 \tag{14}$$

where J is the moment of inertia of the pendulum, a_p is the angular acceleration, m is the pendulum mass, g is the gravitational constant 9.8 m/s^2, l is the distance from the pivot to the center of mass, and α is the angle between the vertical rest position and the pendulum, increasing positively in the clockwise direction.

The energy of the pendulum is the sum of the system's potential and kinetic energy, as described in equation (15), and whose values are zero when α is in an equilibrium position: 0 , $\pm\, \pi$

$$E = \frac{1}{2} J\dot{\alpha}^2 + mgl(1 - \cos \alpha)) = 0 \tag{15}$$

It is essential to grasp the influence of acceleration on the pendulum's energy; by computing the derivative of equation (15), equation (16) is obtained:

$$\dot{E} = J\dot{\alpha}\ddot{\alpha} - mgl\dot{\alpha}\sin\theta = ma_p l\dot{\alpha}\cos\alpha \tag{16}$$

Since the acceleration of the pendulum is proportional to the current supplied to the motor of the arm, just as it is to the voltage, a control law can be established using the following expression identified as equation (17):

$$u = (E - E_0)\dot{\alpha}\cos\alpha \tag{17}$$

where E_0 is a desired energy value. On the other hand, control law (17) can be adjusted to vary the speed at which the energy value E_0 is reached, through a gain . Likewise, the maximum impulse force can be limited by saturating the control signal applied to the motor. All of this is achieved through control law (18):

$$u = sat_{ng}(\mu(E - E_0)sign(\dot{\alpha}\cos\alpha)) \tag{18}$$

The term $sign(\dot{\alpha}\cos(\alpha))$ provides directional information relative to the equilibrium point and enables faster switching in the control action.

As previously mentioned, the goal of the swing-up controller is to drive the system into the region where linear controllers become effective. Within this region, the linear controllers can manipulate the arm angle and, consequently, stabilize the pendulum efficiently.

2.3. State feed-back control

One of the most widely addressed control methodologies in the literature is pole placement control. Its ease of implementation—reduced to a matrix algebra problem—and its effectiveness in operating systems near the equilibrium point make state-feedback control a relevant approach for comparative analysis against model predictive control.

The Furuta pendulum is a system that, in addition to being linearizable depending on the chosen model, can be stabilized around its equilibrium point. Linear control is based on representing the system through linear differential equations or state-space models, with the goal of expressing and identifying the transfer function that underpins the theory [22].

However, the existence of a linear representation does not necessarily imply that the system is controllable using this method. For a system to be controllable under pole placement, it must satisfy the conditions of observability and controllability, ensuring that the full system state can be determined and manipulated from the measured **variables—an** essential requirement for successful linear control [23].

The dynamics of a system can be represented through its state-space equations, which give rise to a canonical control form expressed in equation (19):

$$\begin{aligned} \dot{x} &= Ax + Bu \\ y &= Cx + Du \end{aligned} \tag{19}$$

where A can be represented in its controllable canonical form, diagonal form, or Jordan form, based on a transfer function expressed as in equation (20), in which p corresponds to the system's eigenvalues. As mentioned in [23],the canonical representations of the control equation are shown in equation (21), and the diagonal form is presented in equation (22).

$$\begin{aligned} \frac{Y(s)}{U(s)} &= \frac{b_0 s^n + b_1 s^{n-1} + \cdots + b_{n-1}s + b_n}{S^n + a_1 s^{n-1} + \cdots + a_{n-1}s + a_n} \\ \frac{Y(s)}{U(s)} &= b_0 + \frac{C_1}{s + p_1} + \cdots + \frac{C_n}{s + p_n} \end{aligned} \tag{20}$$

$$\begin{bmatrix} \dot{x_1} \\ \dot{x_2} \\ \vdots \\ \dot{x}_{n-1} \\ \dot{x}_n \end{bmatrix} = \begin{bmatrix} 0 & 1 & 0 & \dots & 0 \\ 0 & 0 & 1 & \dots & 0 \\ \vdots & \vdots & \vdots & \ddots & \vdots \\ 0 & 0 & 0 & \cdots & 1 \\ -a_n & -a_{n-1} & -a_{n-2} & \cdots & -a_1 \end{bmatrix} \begin{bmatrix} x_1 \\ x_2 \\ \vdots \\ x_{n-1} \\ x_n \end{bmatrix} + \begin{bmatrix} 0 \\ 0 \\ \vdots \\ 0 \\ 1 \end{bmatrix} u$$

$$y = \begin{bmatrix} b_n - a_n b_0 & b_{n-1} - a_{n-1} b_0 & \cdots & b_1 - a_1 b_0 \end{bmatrix} \begin{bmatrix} x_1 \\ x_2 \\ \vdots \\ x_n \end{bmatrix} + b_0 u \tag{21}$$

$$\begin{bmatrix} \dot{x}_1 \\ \dot{x}_2 \\ \vdots \\ \dot{x}_n \end{bmatrix} = \begin{bmatrix} -p_1 & 0 & 0 & \cdots & 0 \\ 0 & -p_2 & 0 & \cdots & 0 \\ \vdots & \vdots & \vdots & \ddots & \vdots \\ 0 & 0 & 0 & \cdots & -p_n \end{bmatrix} \begin{bmatrix} x_1 \\ x_2 \\ \vdots \\ x_n \end{bmatrix} + \begin{bmatrix} 1 \\ 1 \\ \vdots \\ 1 \end{bmatrix} u$$

$$y = \begin{bmatrix} c_1 & c_2 & \cdots & c_n \end{bmatrix} \begin{bmatrix} x_1 \\ x_2 \\ \vdots \\ x_n \end{bmatrix} + b_0 u \tag{22}$$

We can transition from the controllable matrix representation (21) to the diagonal form (22),and vice versa, through a transformation. The purpose of expressing them in this way is to simplify the calculation of the characteristic equation, from which the system poles are obtained (23), using the controllable form:

$$|sI - A| = (s - p_1)(s - p_2) \cdots (s - p_n) \tag{23}$$

In order to manipulate the system poles to the desired locations, a variation term is added to the existing matrices, and the system input is canceled, so that the control loop can be represented as shown in Figure 2.

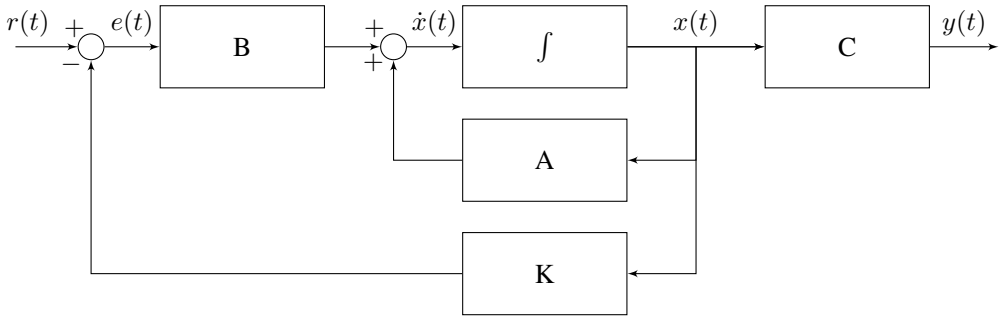

Figure 2. Block diagram for state feedback control. Source: developed by the author.

With $u = Kx$ and $K = [k_1 \;\; k_2 \;\; \cdots \;\; k_n]$ the control equation becomes (24):

$$\dot{x} = Ax + KBx = (A + KB)x \tag{24}$$

From this, the characteristic equation can be obtained, revealing the shift in pole locations due to the presence of K. By leveraging this effect, it is possible to place the poles w as required, provided that K is correctly computed from the desired polynomial.

$$\begin{aligned} EC : \{|sI - (A + KB)| = (s - w_1)(s - w_2)\cdots(s - w_n)\} \\ EC : \{s^n + g_1 s^{n-1} + \cdots + g_{n-1}s + g_n\} \end{aligned} \tag{25}$$

$$EC : \left| SI - \begin{bmatrix} 0 & 1 & 0 & \cdots & 0 \\ 0 & 0 & 1 & \cdots & 0 \\ \vdots & \vdots & \vdots & \ddots & \vdots \\ 0 & 0 & 0 & \cdots & 1 \\ -a_n & -a_{n-1} & -a_{n-2} & \cdots & -a_1 \end{bmatrix} + \begin{bmatrix} 0 \\ 0 \\ \vdots \\ 0 \\ 1 \end{bmatrix} [k_1 \quad k_2 \quad \cdots \quad k_{n-1} \quad k_n] \right| \tag{26}$$

$$EC : \begin{vmatrix} s & -1 & \cdots & 0 \\ 0 & s & \cdots & 0 \\ \vdots & \vdots & \ddots & \vdots \\ a_n + k_n & a_{n-1} + k_{n-1} & \cdots & s + a_1 + k_1 \end{vmatrix} \tag{27}$$

$$\begin{aligned} EC : s^n + g_1 s^{n-1} + \cdots + g_{n-1}s + g_n \\ EC : \quad s^n + (a_1 + k_1)s^{n-1} + \cdots + (a_{n-1} + k_{n-1})s + (a_n + k_n) \end{aligned} \tag{28}$$

By equating the coefficients of the desired polynomial with those of the current one, the constants required for pole relocation can be determined, as shown in equation (28).

In cases where this process needs to be simplified using software, it is advisable to apply the Ackermann method [23], in which the desired polynomial is treated as an extension of matrix A expressed in its controllable canonical form (29).

$$\varphi(A) = A^n + g_1 A^{n-1} + \cdots + g_{n-1}A + g_n \tag{29}$$

By implementing the Ackermann method, the desired constants are obtained from (30).

$$\begin{aligned} K = M \begin{bmatrix} B & AB & \cdots & A^{n-1} & A^n B \end{bmatrix}^{-1} \varphi(A) \\ M = \begin{bmatrix} 0 & 0 & \cdots & 0 & 1 \end{bmatrix} \end{aligned} \tag{30}$$

Although state feedback control is relatively easy to implement, being one of the fundamental strategies in control theory, it provides a baseline for the expected behavior of the controlled system. This, in turn, allows for a meaningful comparison with model-based predictive control.

2.4. Model predictive control

MPC is a control strategy distinguished by its optimization-based nature. As illustrated in Figure 3, the controller operates by predicting the plant's future outputs using the current and past states of the mathematical model, along with optimal control actions obtained by minimizing the reference tracking error.

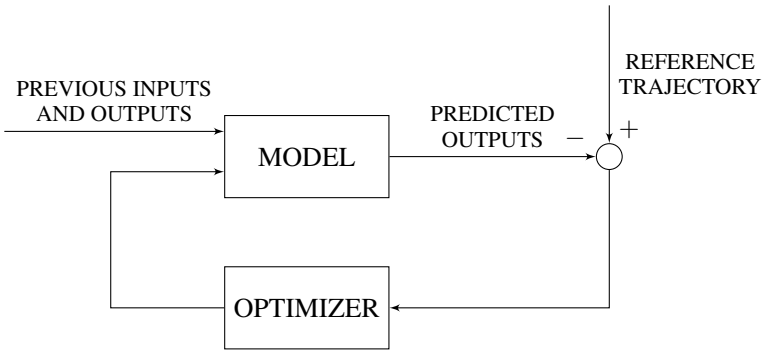

Figure 3. Block diagram of MPC control. Source: developed by the author.

The error minimization function (31), used for reference tracking, is generally defined as proposed in [24]:

$$J = \sum_{i=1}^{N} Q \cdot \left(y(k+i) - y_{ref}(k+i)\right)^2 + \sum_{i=0}^{M} R \cdot \left(\Delta u(k+i)\right)^2 \tag{31}$$

where N is the prediction horizon, representing the number of predicted output steps, $M$is the control horizon, indicating the number of steps over which the input is optimized, Q and R are weighting matrices that penalize the tracking error and control effort, respectively , $y(k+i)$ is the system output at time $k+i$, $y_{ref}(k+i)$ is the desired reference at time $k+i$ and Δu is the variation in the system's control signal(s).

To predict the plant's future outputs, it is necessary to express the governing model in discrete-time state-space form, as shown in (32):

$$\begin{aligned} x(k+1) &= Ax(k) + Bu(k) \\ y(k) &= Cx(k) \end{aligned} \tag{32}$$

where $x(k)$ is the state vector at time k, $y(k)$ is the system output vector, ,and $u(k)$is the control vector containing the system inputs A, B and C are the discrete matrices that describe the system dynamics in state-space form.

The sequence of future outputs can be written in matrix form as shown in (33):

$$\mathbf{y} = \begin{bmatrix} y(k+1) \\ y(k+2) \\ \vdots \\ y(k+N) \end{bmatrix} = \begin{bmatrix} C \\ CA \\ \vdots \\ CA^{N-1} \end{bmatrix} x(k) + \begin{bmatrix} CB & 0 & \cdots & 0 \\ CAB & CB & \cdots & 0 \\ \vdots & \vdots & \ddots & \vdots \\ CA^{N-1}B & CA^{N-2}B & \cdots & CB \end{bmatrix} \mathbf{u} \tag{33}$$

Naming the matrix that multiplies $x(k)$ as Φ, and the matrix that multiplies u as S, as done in [25], the system output prediction equation—based on the inputs and the current and past states—is expressed in (34):

$$y = \Phi x(k) + S\mathbf{u} \tag{34}$$

On the other hand, y_{ref} is a $1xN$ vector, such that the cost function J,in matrix form, is defined as shown in (35):

$$J = \left(y_{ref} - (\Phi\, x(k) + Su)\right)^T Q \left(y_{ref} - (\Phi x(k) + Su)\right) + u^T R u \tag{35}$$

The control vector is obtained by minimizing J, through the derivative of J with respect to u set equal to zero, under the assumption of an unconstrained optimization problem. In this way, the values of the control vector are given by (36):

$$Q\left(y_{ref} - \Phi x(k)\right) u = \left(S^T Q S + R\right)^{-1} S^T \tag{36}$$

Only the first value of the resulting control vector u is applied to the system. This control signal computation is repeated at each time step.

2.5. Swing-up control design

The controller designed to perform the pendulum swing-up is the one presented in the QUANSER pendulum guide [26], where the swing amplitude is defined by the parameters μ, E_r and a_{pmax} initially ensuring swing-up with amplitudes below 90, based on the guide's suggested values as follows: $\mu = 50\frac{m}{s^2 J}$, $E_r = 10mJ$ and $a_{pmax} = 12\frac{m}{s^2}$,due to the high sensitivity of the swing-up control with respect to μ. This parameter is used to scale the swing amplitude beyond the levels defined by the reference energy. Accordingly, the approach to the linear region is first adjusted by increasing μ, and the final entry into the linear region is refined by increasing the reference energy. Through the implementation of these parameters and experimentation with the system, the following values were obtained: $\mu = 55\frac{m}{s^2 J}$, $E_r = 13\ mJ$ and $a_{pmax} = 12\frac{m}{s^2}$. The resulting behavior enables a steadily ascending swing-up that reaches the boundaries of the linear region, as demonstrated in Figure 4.

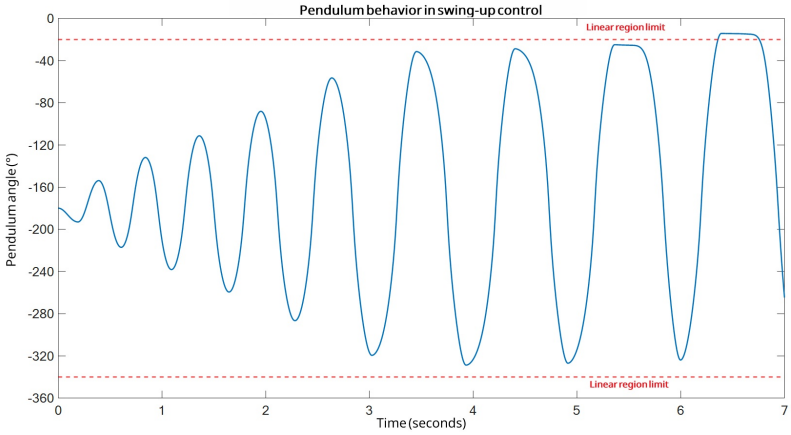

Figure 4. Swing-up control behavior in the Furuta pendulum. Source: developed by the author.

2.6. Hybrid control design

Hybrid control is a technique that combines swing-up and stabilization strategies through controller switching. This combination is employed due to the nonlinear nature of the system, particularly considering the pendulum's angular position. To implement it, specific operating regions are defined for each controller, as illustrated in Figure 5 and as recommended by the manufacturer in the QUANSER control guide [26].

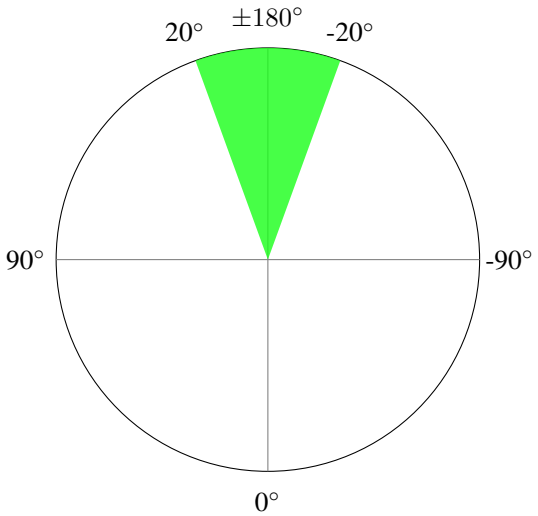

Figure 5. Operating regions for hybrid control. Source: developed by the author.

The green-shaded region corresponds to the operating zone of the stabilization controller, while the unshaded section represents the swing-up controller's domain. Figure 6 shows the block diagram of the complete hybrid control system for the Furuta pendulum.

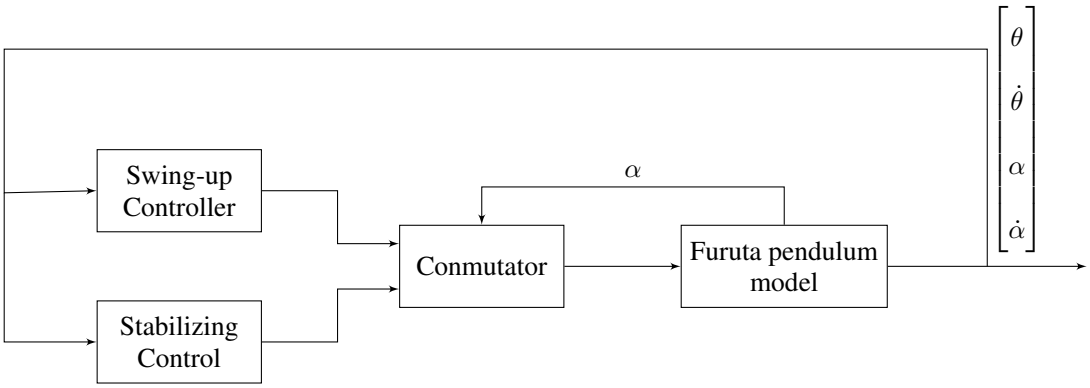

Figure 6. Block diagram of the hybrid controller. Source: developed by the author.

2.7. *Controller design at the equilibrium point*

The designed controllers must maintain the pendulum in an upright inverted position (α = 180°) while simultaneously tracking the reference position of the rotary arm. In the Quanser QUBE Servo 2 test system, the latter is physically constrained to a θ range between 90 and -90, with the system used in the experiments shown in Figure 7:

Figure 7. Experimental setup of the physical test system used for controller validation. Source: developed by the author

2.7.1. Pole placement control The control system implemented using the pole placement technique is shown in Figure 8.

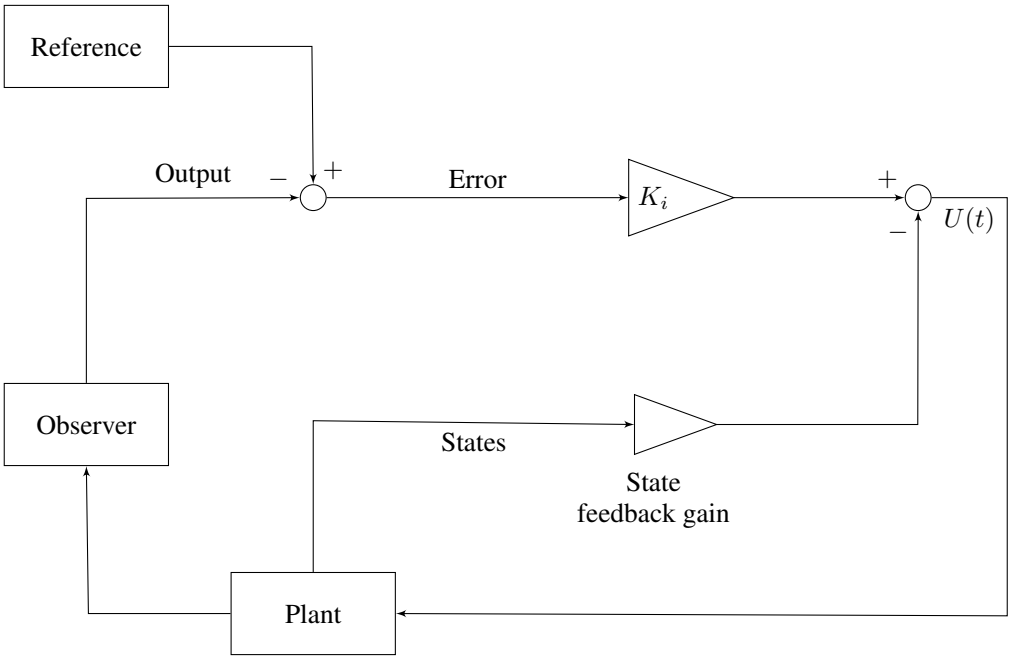

Figure 8. Block diagram of the implemented pole placement control. Source: developed by the author.

To compute the state feedback gains, the poles indicated in 37 were selected. These were determined based on experimental analysis of the pendulum, initially using the pole locations implemented in [1],and considering the system's good performance once the pendulum reaches the linear region.

$$P = \begin{bmatrix} 7.5 & -8.25 & -9 - 1.5i & -9 + 1.5i \end{bmatrix} \tag{37}$$

On the other hand, the pole associated with the integral gain K_i was set to -18. Consequently, the state gains and K_i, obtained through pole placement, are presented in 38.

$$P = \begin{bmatrix} -8.603 & 1.9729 & 35.1082 & 3.0066 & 16.3457 \end{bmatrix} \tag{38}$$

2.7.2. Model predictive control The MPC control system implemented in this study is shown in Figure 9.

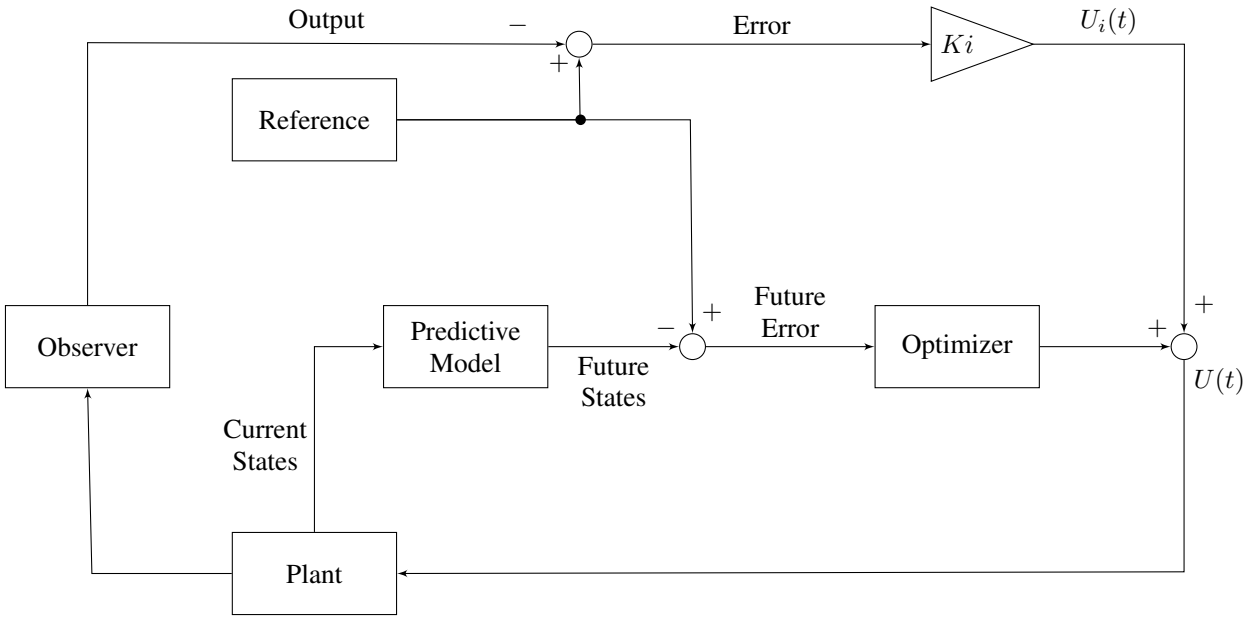

Figure 9. Block diagram of the implemented MPC. Source: developed by the author.

Starting from the fact that the model used to describe the physical behavior of the plant is not perfect since, compared to the real plant, it does not account in detail for variables such as friction an uncertainty is introduced into the employed linear predictive model. This model can be adjusted through the configuration of the prediction and control horizons. Nevertheless, MPC controllers provide a margin of operability against such uncertainties, which can be mitigated through appropriate tuning of the control parameters, as indicated in [27].

In this context for the predictive model shown in Figure 9, a discretization time T_s of 0.01 seconds is established. Using the linearized system values from 13 the resulting discrete-time system is obtained in (39), It is important to note that this sampling time directly affects the control and prediction horizons N and M, as well as the weighting matrices Q and R, since a different T_s would yield a discrete system with different characteristics:

$$F_{discrete}: \begin{bmatrix} X_1 \\ X_2 \\ X_3 \\ X_4 \end{bmatrix} = \begin{bmatrix} 1 & 0.0099 & 0.0074 & 0 \\ 0 & 0.9793 & 1.4837 & 0.0074 \\ 0 & -0.001 & 1.0131 & 0.01 \\ 0 & -0.0205 & 2.6121 & 1.0131 \end{bmatrix} \begin{bmatrix} x_{l1} \\ x_{l2} \\ x_{l3} \\ x_{l4} \end{bmatrix} + \begin{bmatrix} 0.0025 \\ 0.4933 \\ 0.0024 \\ 0.4885 \end{bmatrix} \tag{39}$$

The selection of the prediction horizon N and the control horizon M, as well as the weighting matrices Q and R, was carried out through a manual tuning process focused on balancing accuracy, stability, and computational efficiency. To this end, the prediction horizon started from a low initial value ($N = 5$), with progressive increments of 5, until achieving a steady-state error within $\pm 1^{\circ}$ in the pendulum arm. According to [28], a longer horizon ensures that the optimization process considers a broader predictive window of the system dynamics, thereby improving steady-state performance, albeit at the expense of increased computational load.

On the other hand, M was set to 30, a value consistent with the recommendation in [28] where it is suggested to initially set $M = N$. The parameter was then systematically reduced in steps of 5 through performance tests in order to decrease the aggressiveness of control actions, while still maintaining a sufficiently fast response to reference tracking without compromising either stability or response time due to excessive computational effort.

The initial values of Q and R were 200 and 1, respectively. The main objective was to achieve a more accurate response without destabilizing the system and to avoid overshoot. To this end, the Q-to-R ratio was significantly increased. The iterative tuning methodology, validated through comparison with a state-feedback controller, demonstrated that the final configuration ($N = 45, M = 30, Q = 500, R = 0.5$) meets the performance requirements, achieving a steady-state error

within the specified margin ($\pm 1^{\circ}$). This approach ensures that the predictive controller attains suitable dynamic behavior and fulfills the design specifications for high-precision position control applications.

On the other hand, to eliminate steady-state error, integral action was incorporated as a separate loop external to the MPC formulation. Specifically, the tracking error $e(t) = r(t) - y(t)$ was integrated, and the resulting integral state was multiplied by a gain $K_i = -5$.

The currently proposed switching scheme in the hybrid control primarily affects the MPC, due both to the convergence considerations of the linear model on which the prediction is based and to the presence of implicit variables in the actual system behavior that are not captured by the base model. In the linearization process, approximations such as $\sin(\alpha) \approx \alpha$ and $\cos(\alpha) \approx 1$ are employed, which are only valid within a limited range of angles. The linear controller begins to act at angular values close to this validity limit, which causes the predicted error to exhibit greater uncertainty during these transitions compared to the error computed closer to the upper equilibrium point—the reference used for the linearization. This error is compensated by the feedback action of the controller, though at the cost of increased settling times during the initial switching between controllers [27].

MPC, when employing a linear predictive model, exhibits sensitivity to the variables around which the linearization was performed. This opens the possibility, in future work, of improving its performance through strategies that adapt those variables to which the predictive model is most sensitive. In the literature, different approaches have been proposed: on the one hand, the incorporation of a dead zone within the angular range between the swing-up and the linear region, so that no control action is applied in this interval, thereby reducing the inertia with which the system enters the switching stage to MPC [1]. On the other hand, within this same transition range, an active control strategy can be applied to modulate the inertia to a specific value before switching.

Additionally, by exploiting the sensitivity of the predictive model to the linearization point, it is possible to segment the operating range of the plant into several linearized models around different operating points. In this scheme, the controller switches between these predictive models and their respective optimizations, a configuration that has been developed and simulated in [29].

2.8. ITAE index

To evaluate controller performance, it is not sufficient to analyze the system's dynamic behavior graphically; performance must also be quantified through metrics such as settling time, overshoot, and system error. In this context, the Integral of Time multiplied by the Absolute Error (ITAE) criterion is particularly useful for assessing controller performance. This metric is implemented as described in [30], and is defined by (40):

$$\int_0^{\infty} t|E(t)|\,dx \tag{40}$$

3. Results

This section presents the results of the experimental tests conducted on the QUANSER QUBE Servo 1 inverted pendulum system using the previously described controllers. The tests evaluated the performance of the rotary arm in three scenarios: stabilization with a fixed reference and rejection of disturbance, tracking of a step-varying reference, andtracking of a sinusoidal reference. Each test was conducted over a 70-second interval, sufficient to observe both transient and steady-state responses.

The results are organized into three main categories: Physical behavior, analyzing mechanical variables such as the arm and pendulum angles. Electrical behavior, focusing on signals related to control effort. Performance indices, quantifying controller effectiveness using a standardized metric. The results reported are based on a single run; however, actual implementation may exhibit performance variations.

3.1. Results of the physical behavior of the system

In this section, the response of the system's physical variables is obtained, initially tested with a fixed reference input of 0, and subjected to short-duration disturbances. From this first test, Figure 10 is obtained, which is used to evaluate the recovery capability and disturbance rejection of each proposed control structure. To ensure fair comparison conditions, a low-magnitude signal is injected directly into the pendulum angle measurement within the Simulink control scheme. This modification allows observation of how both controllers respond to a sudden system disturbance while maintaining a constant reference.

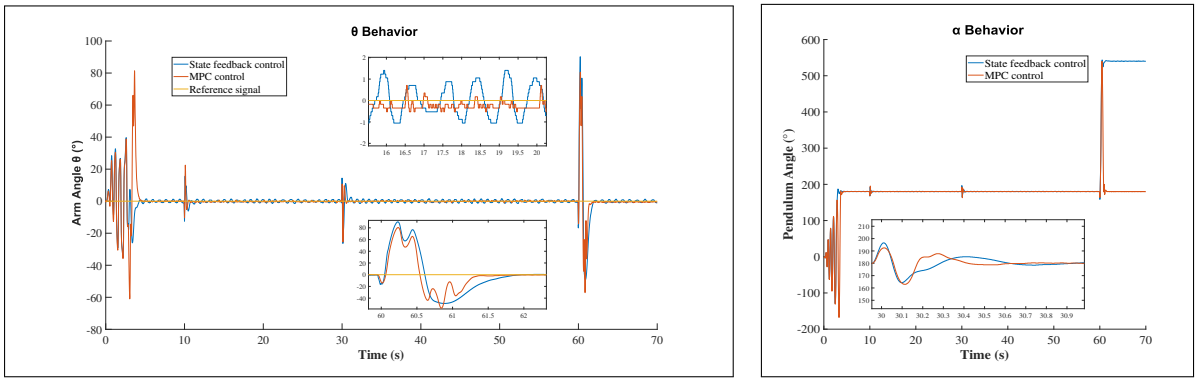

(a) (b)

Figure 10. System behavior under a constant reference with applied disturbances: **a)** Arm position. **b)** Pendulum position. Source: developed by the author.

From this initial test, the MPC controller exhibited a smaller steady-state tracking error and, on average, a $0.370\ s$ faster response compared to the state feedback controller when subjected to disturbances, as quantified in Table 3. While the MPC performed well in the steady-state region and in disturbance rejection, its most unfavorable condition occurred during the pendulum's swing-up from its initial position. In this phase, it required more time to bring the pendulum into the equilibrium zone compared to the state feedback controller, this is attributed to limitations of the linear model and the corrective signals predicted by the controller.

Table 3. Stabilization Times in the System Using a Stable Reference and Applying Disturbances

Disturbance Start Time (s)	**MPC Control (s)**	**State-Feedback Control (s)**
9.950	0.694	0.808
29.955	0.769	1.484
59.942	1.753	2.037

Although the robustness of the control schemes has been evaluated, characterizing their performance also requires assessing responsiveness across different operating ranges. Figure 11 shows the behavior of the arm and pendulum angles in response to a periodic step reference signal ranging from 50 to -50. This operating window allows for the analysis of key indicators such as settling time during each transition.

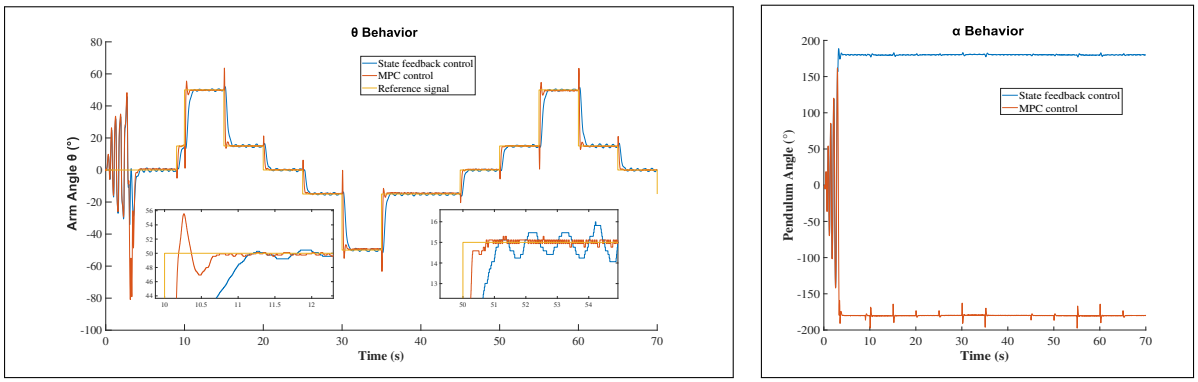

(a) (b)

Figure 11. System behavior under a step reference input: **a)** Arm position. **b)** Pendulum position. Source: developed by the author.

The most significant observable feature in Figure 11 is the change in the nature of the system's response. The state feedback controller produces an overdamped response, resulting in longer settling times, whereas the MPC controller yields an under-damped response, allowing the system to reach equilibrium more quickly. This difference not only affects response times but also directly impacts the energy levels required by each control strategy.

Across all reference amplitude variations, the MPC controller consistently outperforms the state feedback controller in terms of settling time, with an average improvement of approximately $2.5\ s$. Moreover, the MPC demonstrates strong operational versatility across different reference ranges once the equilibrium point is reached at α, as evidenced by a standard deviation of $0.146\ s$, indicating that settling times remain close to the average. In contrast, the state feedback controller exhibits greater variability, with a standard deviation of $1.69\ s$. As shown in the data collected in Table 4, no clear trend is observed in the settling time range: in some cases, it takes up to $4\ s$, while in others it takes less than $1\ s$, even when near the equilibrium point at α. This positions the MPC controller as the more consistent option.

Table 4. Stabilization Times in the System Using a Step Reference

Interval	Reference Signal Amplitude (°)	State-Feedback Control (s)	MPC Control (s)	Difference (s)
1	0	7.193	4.071	3.122
2	15	0.921	0.292	0.629
3	50	1.078	0.628	0.450
4	15	4.229	0.609	3.620
5	0	4.373	0.559	3.815
6	-15	0.902	0.317	0.585
7	-50	1.792	0.656	1.136
8	-15	4.178	0.562	3.616
9	0	0.886	0.290	0.596
10	15	0.913	0.289	0.624
11	50	1.071	0.650	0.421
12	15	4.062	0.599	3.463
13	0	4.798	0.299	4.499

Unlike the characteristics evaluated in previous tests, Figure 12 is used to detail the response speed of each control scheme. It illustrates the behavior of the arm and pendulum angles when the system is subjected to a sinusoidal reference signal with an amplitude of 90° and a frequency of $0.5\frac{rad}{s}$.

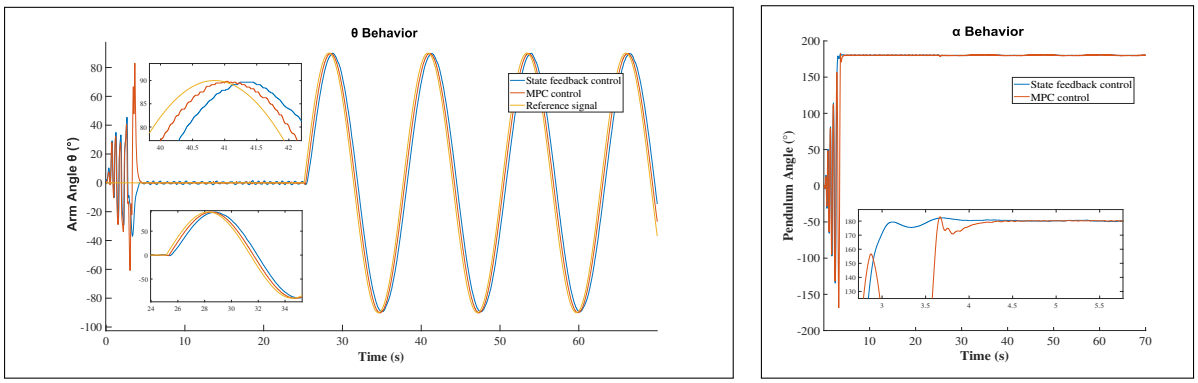

(a) (b)

Figure 12. System behavior under a sinusoidal reference input: **a)** Arm position. **b)** Pendulum position. Source: developed by the author.

Highlighting the most prominent feature observed in the previous two tests, the system with MPC control exhibits faster response under the sinusoidal reference, with a delay of 200-210 ms relative to the reference signal, approximately 290 ms shorter than the response of the state feedback controller, which shows a delay of 500-520 ms. This temporal performance difference is characterized based on the trend of the data presented in Table 5.

Table 5. Time Values Used by the System When Tracking a Sinusoidal Reference

Signal of Arm Angle	First Zero Crossing		Second Negative Peak		Fourth Positive Peak	
	Amplitude	Time (s)	Amplitude	Time (s)	Amplitude	Time (s)
Reference	0	31.415	-90.0000	47.125	89.9990	65.983
MPC Control	0	31.642	-90.1758	47.299	89.6484	66.196
State-Feedback Control	0	31.932	-89.2969	47.584	89.6484	66.508

3.2. Results of the system's electrical behavior

As a fundamental part of the comparison process between both controllers, the voltage values required by each control strategy during the tests are analyzed below. Figures 13 through to Figure 15 present both general and detailed views of the timing and magnitude of the voltage demand. This analysis provides complementary insight into the performance of the control strategies, since although both may deliver adequate dynamic behavior, the control signals can reveal differences in control effort, magnitude, and energy consumption

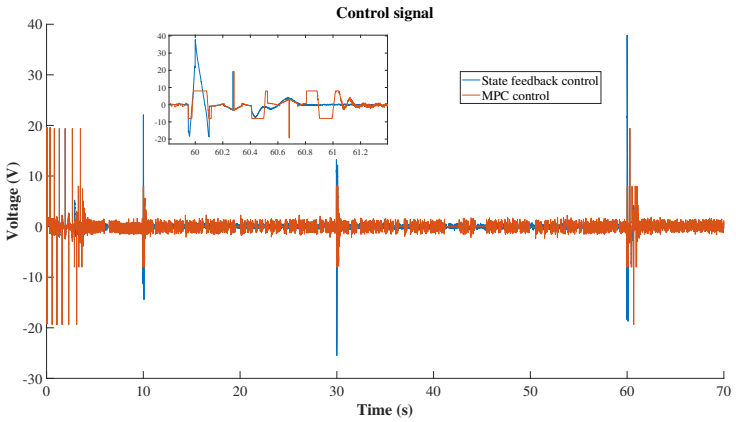

Figure 13. Control signal under constant reference with disturbances. Source: developed by the author.

Figure 13 shows higher energy consumption in the steady state by the MPC controller, a behavior associated with its fast and precise response. In contrast, when correcting a disturbance, the state feedback controller demands more voltage without achieving a faster correction time compared to the MPC controller, highlighting the anticipatory nature of the latter.

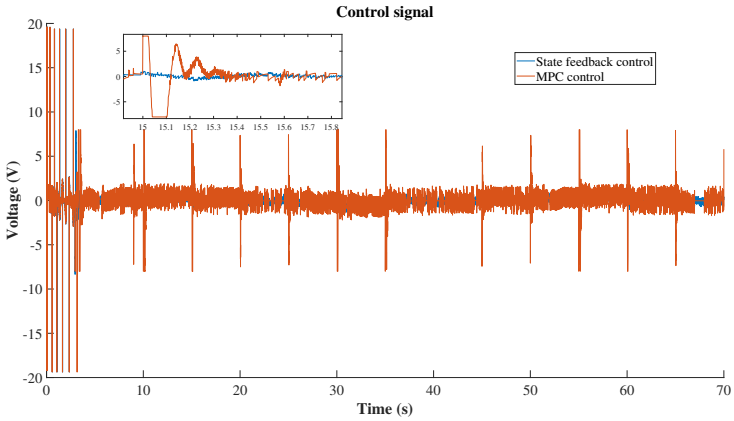

Figure 14. Control signal under step-type variable reference. Source: developed by the author

Figure 14 corresponds to the step-response test, where it is evident that the MPC controller applies more aggressive and faster corrections to maintain the desired reference. This results in overall better performance and a higher correction speed in response to reference changes.

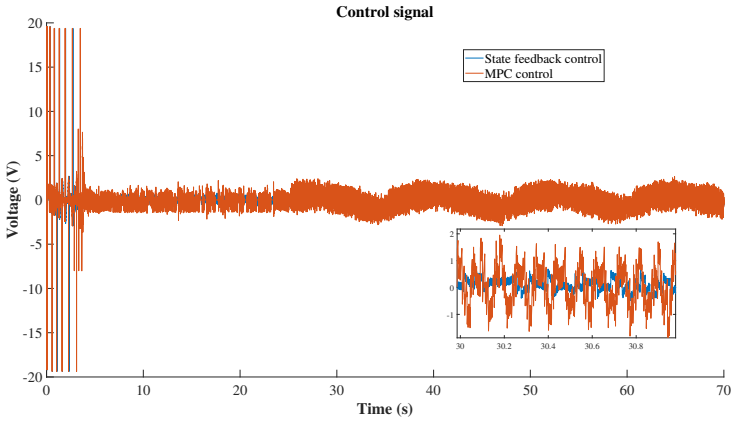

Figure 15. Control signal under sinusoidal reference input. Source: developed by the author.

In Figure 15, corresponding to the sinusoidal test, the same behavior of greater amplitude and frequency in the response of the MPC controller is observed, resulting in a shorter delay in control action relative to the reference signal. In general terms, the MPC controller exhibited the highest voltage demand due to the rapidity of its control actions. However, this behavior did not persist under steady-state disturbances, where the linear controller required a larger signal amplitude. Despite this increased demand, the state feedback strategy responded more slowly than the MPC, further highlighting the predictive capability of the latter.

3.3. System error results

The ITAE criterion is used to evaluate the performance of both controllers, as it penalizes errors over time, assigning greater weight to persistent deviations. Figures 16 through Figure 18 show the evolution of the accumulated ITAE over time for both the state-feedback and the MPC controllers.

Based on the disturbance rejection test and the performance index analysis shown in Figure 16,the MPC controller demonstrated favorable behavior. This is reflected in a shallower slope in the ITAE curve, indicating faster recovery from disturbances and a greater reduction in accumulated error over time. Moreover, MPC contributed less to the growth of the ITAE after each disturbance, underscoring its ability to mitigate the effects of perturbations. In contrast, the state-feedback controller exhibited 54% more accumulated error than MPC by the end of the 70-second test.

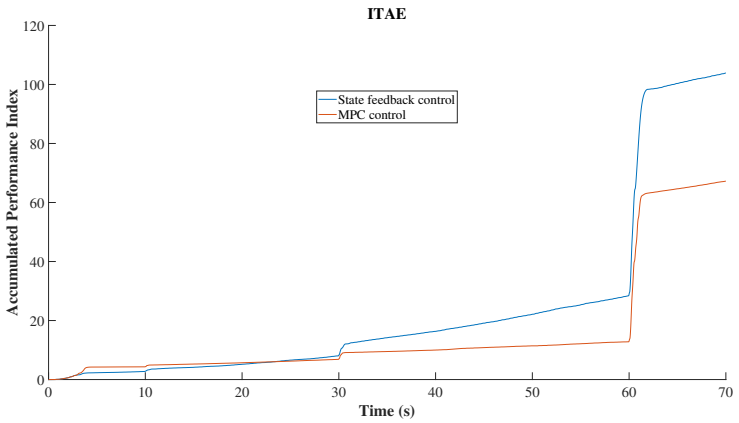

Figure 16. Cumulative error under constant reference with disturbances. Source: developed by the author.

Considering the versatility of the MPC controller, demonstrated in previous results through its effective performance across various reference values, Figure 17 illustrates the ITAE of the system's response to a step reference signal. Unlike the state feedback controller, the MPC exhibits steeper slopes with each reference change, highlighting its responsiveness. The figure also reveals the limitations of the state feedback controller when handling reference changes greater than 10,where the performance index increases significantly—resulting in a value 112% higher than that of the MPC controller after 70 seconds of testing.

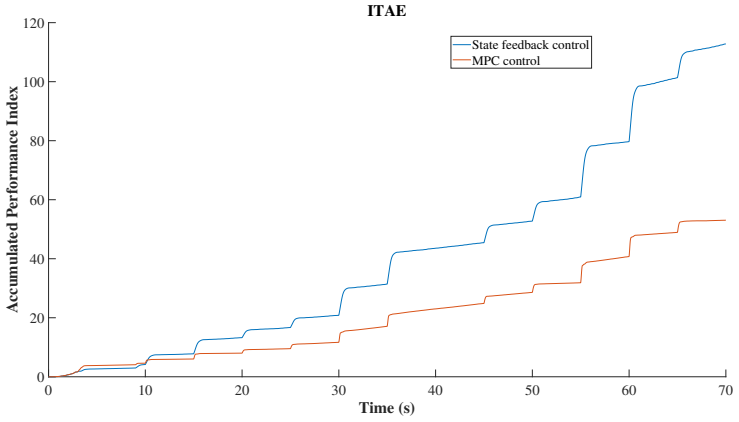

Figure 17. Cumulative error under step-type variable reference. Source: developed by the author.

In the comparative analysis of the control schemes, the MPC controller demonstrates its greatest advantage over the state feedback controller in tracking time-varying references. This behavior is further illustrated in Figure 18, where the accelerated and continuous growth of the cumulative error is more clearly observed, with a nonlinear trend in both control strategies. Although both attempt to follow the reference signal, a delay is present in the system's response under each controller, resulting in greater penalization during each cycle. Consequently, the controller with the larger phase lag relative to the reference also accumulates a higher ITAE value.

Under this dynamic condition, the ITAE of the state feedback controller is 124% higher than that of the MPC, representing the most significant difference between the two across the three tests conducted. It is worth noting that this disparity tends to be more pronounced in scenarios involving variable references, as opposed to those with constant reference signals.

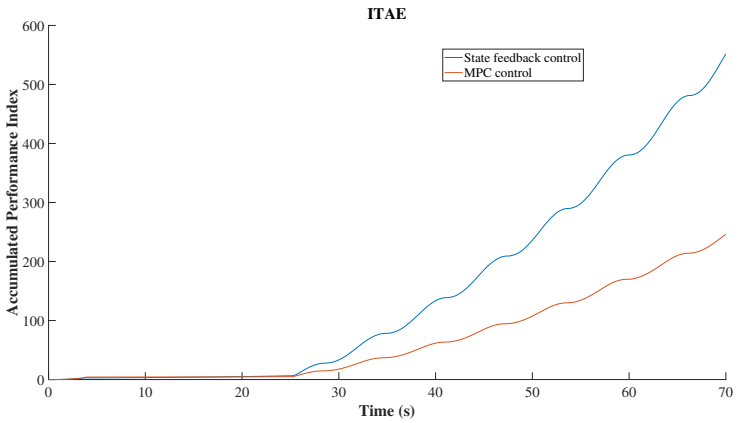

Figure 18. Cumulative error under sinusoidal reference input. Source: developed by the author.

Overall, the results indicate that the MPC controller exhibits a lower cumulative error throughout the entire time interval analyzed—except during the initial seconds, due to its switching limitations. Additionally, the slope of the ITAE curve for the state feedback controller is steeper, indicating that the weighted error continues to grow at a higher rate compared to the MPC. This suggests that the MPC handles the system dynamics more effectively, reducing state errors. When observing the index across different time intervals in the three tests as shown in Table 6, the MPC consistently maintains the lowest value, despite having shown some difficulty in bringing the pendulum to the equilibrium point faster than the state feedback controller.

Table 6. Performance Criterion Values

Scenario	**ITAE (θ) in** $20\ s$		**ITAE (θ) in** $50\ s$		**ITAE (θ) in** $70\ s$	
	MPC	**State Feedback**	**MPC**	**State Feedback**	**MPC**	**State Feedback**
Constant Reference + Disturbances	5.6881	5.1783	11.4237	22.1259	67.246	103.92
Step Reference	8.0098	13.2535	28.6802	52.8325	53.0608	112.7801
Sinusoidal Reference	4.57657	4.98632	107.509	236.219	246.333	551.792

4. Conclusions

This study presented the implementation and experimental analysis of an inverted pendulum system using identical modeling parameters and the same swing-up strategy, while alternating the stabilization approach between state-feedback control and MPC.

It was observed that during t he initial stages of the system's dynamics, the state-feedback controller exhibited better performance, particularly in the moments preceding the controller switch. This advantage was partly due to the absence of an inertia-reduction zone in the predictive model, which should account for the specific limitations and conditions under which the model was developed. In fact, the predictive model was designed to represent behavior with lower inertia, closer to the equilibrium point.

However, once the system entered the linear control region, the MPC controller significantly improved its performance, demonstrating advantages in error reduction, disturbance rejection, and response speed. In all three tests conducted, MPC showed superior overall behavior, particularly in tracking variable references—even as the frequency of changes increased. Nevertheless, this improved performance came at the cost of higher voltage requirements and the appearance of overshoot in response to step references.

Overall, the results highlighted the predictive controller's ability to reduce accumulated error, attributable to its capacity to anticipate system evolution and optimize control actions accordingly.

For future work, it is recommended to incorporate more appropriate constraints into the optimization problem to further enhance MPC performance, especially when considering actuator limitations. Additionally, the inclusion of an inertiareduction or "dead zone" or or implement several predictive models segmented over an operating range beyond the equilibrium point could facilitate smoother transitions between switched controllers. Experimental practices should also be strengthened by repeating tests and reporting average metrics with standard deviations. Additionally, analyzing power consumption or total energy usage would quantitatively support the observation that MPC performance often comes at an energy cost. The effect of voltage saturation on stability should be further examined, with hardware-level protections (e.g., current-limiting circuits) considered. Exploring adaptive horizons, data-driven model updates, and deployment on embedded platforms such as Raspberry Pi would provide valuable insights into real-world applicability. Finally, Implement a velocity-based switching criterion (e.g., transition only when $|\dot{\alpha}| <$ threshold near equilibrium) or hysteresis band to reduce chattering.

5. Acknowledgments and foundings

This research was supported by the Ibero-American Program for Science and Technology for Development (CYTED) through the thematic network 723RT0150, Network for the Large-Scale Integration of Renewable Energy into Power Systems (RIBIERSE-CYTED).

To God, who opens the doors to scientific knowledge and enlightens us to achieve our goals. Generative AI tools also contributed to refining the manuscript's writing and structure. These improvements were entirely based on the authors' original ideas, ensuring clarity and coherence in the presentation of the research findings.

Author's conflicts of interest

The authors declare no conflicts of interest.

Author's Contributions

Oscar Danilo Montoya-Giraldo: Conceptualization, formal analysis, investigation, writing, review, and editing. Sebastián David Pintor Ahumada: Conceptualization, formal analysis, assembly, investigation, methodology, simulation, original draft writing, and review. Camilo Esteban Pérez Espíndola: Conceptualization, formal analysis, investigation, assembly, methodology, simulation, original draft writing, and review.

REFERENCES

1. Luisa F. Escobar-Dávila, Oscar D. Montoya-Giraldo, and Didier Giraldo-Buitrago. Control global del péndulo de furuta empleando redes neuronales artificiales y realimentación de variables de estado. *TecnoLógicas*, (30):71, June 2013.
2. SHOZO MORI, HIROYOSHI NISHIHARA, and KATSUHISA FURUTA. Control of unstable mechanical system control of pendulum†. *International Journal of Control*, 23(5):673–692, May 1976.
3. Nicholas J. Jensen and Takayuki Ishizaki. Furuta Pendulum Design Update for Accessible Control Demonstrations. *IFAC-PapersOnLine*, 56(2):7573–7578, 2023.
4. M. Yamakita, K. Furuta, K. Konohara, J. Hamada, and H. Kusano. Vss adaptive control based on nonlinear model for titech pendulum. In *Proceedings of the 1992 International Conference on Industrial Electronics, Control, Instrumentation, and Automation*, pages 1488–1493. IEEE, 2003.
5. Mayra Antonio-Cruz, Victor Manuel Hernandez-Guzman, Carlos Alejandro Merlo-Zapata, and Celso Marquez-Sanchez. Nonlinear control with friction compensation to swing-up a furuta pendulum. *ISA Transactions*, 139:713–723, August 2023.
6. Fuzzy Swing Up Control and Optimal State Feedback Stabilization for Self-Erecting Inverted Pendulum. *IEEE Access*, 8:6496–6504, 2020.
7. Xinrong Zhang, Jie Ma, Lian Lin, and Lele Wang. Study on swing-up control of rotary inverted pendulum based on energy feedback. In *2018 5th International Conference on Information Science and Control Engineering (ICISCE)*, pages 994–998. IEEE, July 2018.
8. Ewelina Cholodowicz and Przemyslaw Orlowski. Optimization of a fractional order controller for the furuta pendulum with an output disturbance using a genetic algorithm. In *2022 17th International Conference on Control, Automation, Robotics and Vision (ICARCV)*, pages 373–379. IEEE, December 2022.
9. Ngo Phong Nguyen, Hyondong Oh, Yoonsoo Kim, and Jun Moon. A nonlinear hybrid controller for swinging-up and stabilizing the rotary inverted pendulum. *Nonlinear Dynamics*, 104(2):1117–1137, 2021.
10. Ricardo Binz and Stanislav Aranovskiy. Iterative learning control strategy for a furuta pendulum system with variable-order linearization. *IFAC-PapersOnLine*, 54(20):14–19, 2021.
11. David Acosta Villamil, Jovanny Pacheco Bolivar, Jose Noguera Polania, and Marco Sanjuan Mejia. Neural network armax model for a furuta pendulum. *Ingeniare. Revista chilena de ingeniería*, 29(4):668–682, December 2021.
12. Wilber Acuña-Bravo, Andrés Guillermo Molano-Jiménez, and Enrico Canuto. Embedded model control for underactuated systems: An application to Furuta pendulum. *Control Engineering Practice*, 113(May):12, 2021.
13. Mate B. Vizi and Gabor Stepan. Stability of the furuta pendulum with delayed digital controller. *IFAC-PapersOnLine*, 54(18):204–208, 2021.

14. G. Rigatos, P. Siano, M. Abbaszadeh, S. Ademi, and A. Melkikh. Nonlinear h-infinity control for underactuated systems: the furuta pendulum example. *International Journal of Dynamics and Control*, 6(2):835–847, August 2017.
15. Max Schwenzer, Muzaffer Ay, Thomas Bergs, and Dirk Abel. Review on model predictive control: an engineering perspective. *The International Journal of Advanced Manufacturing Technology*, 117(5–6):1327–1349, August 2021.
16. L. R. C. Moura, M. A. F. Montezuma, M. Mendonça, R. H. C. Palácios, C. R. A. Oliveira, A. N. Vargas, M. A. Diop, and R. Breganon. Controlling the furuta pendulum: Proof of concept through virtual prototyping. *Journal of Applied Research and Technology*, 22(3):327–335, June 2024.
17. Victor Manuel Hernández-Guzmán and Ramón Silva-Ortigoza. *Control of a Furuta Pendulum*, pages 869–919. Springer International Publishing, September 2018.
18. Anjana Govind and S. Selva Kumar. *A Comparative Study of Controllers for QUANSER QUBE Servo 2 Rotary Inverted Pendulum System*, pages 1401–1414. Springer Singapore, 2020.
19. Ahmad Taher Azar and Quanmin Zhu, editors. *Advances and Applications in Sliding Mode Control systems*. Springer International Publishing, 2015.
20. Mukhtar Fatihu Hamza, Hwa Jen Yap, and Imtiaz Ahmed Choudhury. Cuckoo search algorithm based design of interval type-2 fuzzy pid controller for furuta pendulum system. *Engineering Applications of Artificial Intelligence*, 62:134–151, June 2017.
21. Alvaro Prado, Marco Herrera, and Oswaldo Menéndez. Intelligent swing-up and robust stabilization via tube-based nonlinear model predictive control for a rotational inverted-pendulum system. *Revista Politécnica*, 45(1):49–64, April 2020.
22. Li Zhang and Roger Dixon. Robust nonminimal state feedback control for a furuta pendulum with parametric modeling errors. *IEEE Transactions on Industrial Electronics*, 68(8):7341–7349, August 2021.
23. Arturo Cruz Avilés, Martín Ortiz Domínguez, and Yira Muños-Sánchez. Ingeniería de control moderna. *Ingenio y Conciencia Boletín Científico de la Escuela Superior Ciudad Sahagún*, 5(10), July 2018.
24. Basil Kouvaritakis and Mark Cannon. *Model Predictive Control*. Springer International Publishing, 2016.
25. Juan Libardo Duarte Madrid, E.A. Gonzalez Querubin, and P.A. Ospina-Henao. Predictive control of a furata pendulum. In *2017 IEEE 3rd Colombian Conference on Automatic Control (CCAC)*, pages 1–6. IEEE, October 2017.
26. Freeman. *Instructor Workbook*, volume 53. 2013.
27. Changrui Liu, Shengling Shi, and Bart De Schutter. Stability and performance analysis of model predictive control of uncertain linear systems. *IEEE*, pages 7356–7362, 2024.
28. Mohammed Alhajeri and Masoud Soroush. Tuning guidelines for model-predictive control. *Industrial & Engineering Chemistry Research*, 59(10):4177–4191, February 2020.
29. Jue He, Yongbo Li, Ziang Wei, and Zixin Huang. Gain-scheduled model predictive control for cart–inverted-pendulum with friction and disturbances. *Applied Sciences*, 13(24):13080, December 2023.
30. Jesus Dario Mina Antonio, Eduardo Miramón Juarez, Oscar Hernández Martínez, and Miguel Francisco Sabido Borges. Diseño optimizado del conjunto filtro-controlador de un inversor para mejorar su integración a red. *Ingeniería Investigación y Tecnología*, 23(4):1–13, July 2022.